Phosphate removal using aluminum-doped magnetic nanoparticles

Jie Xu[a,*], Letitia Luu[a], Yuanzhi Tang[b]

[a]*Aerospace, Transportation and Advanced Systems Laboratory, Georgia Tech Research Institute, Georgia Institute of Technology, Strong St, Atlanta, GA 30318, Tel. 404-407-6122; email: jie.xu@gtri.gatech.edu (J. Xu), letitialuu@gmail.com (L. Luu)*
[b]*School of Earth and Atmospheric Sciences, Georgia Institute of Technology, 311 Ferst Drive, Atlanta, GA 30332-0340, Tel. 404-894-3814; email: yuanzhi.tang@eas.gatech.edu*

ABSTRACT

Modern industrial waste waters often contain high concentrations of phosphate, and many methods have been explored to aid in its removal. This study investigates the use of magnetic nanoparticles as an adsorbent for phosphate removal. Aluminum-doped magnetic nanoparticles were synthesized using a co-precipitation method. Structure and composition analysis of the prepared magnetic nanoparticles indicated an inverse spinal structure with a composition of $FeAl_{0.75}Fe_{1.25}O_4$. These nanoparticles were tested for their phosphate removal properties, including adsorption capacity, selectivity, and kinetic models. They showed great affinity to phosphate with a maximum adsorption capacity of 102 mg/g. Additionally, the adsorption was selective, and the presence of other common anions and organic matters did not interfere with the phosphate adsorption efficacy. The kinetic analysis of phosphate adsorption suggested a pseudo-second-order adsorption behavior, and the adsorption isotherm studies indicated a Langmuir type adsorption. The phosphate removal capabilities of the nanoparticles were also tested in poultry rinsing water, tap water, and municipal wastewaters, all with high phosphate removal efficiency. The overall results from these experiments showed promising results for the phosphate removal efficacy of these nanoparticles.

Keywords: Phosphate; Adsorption; Magnetic nanoparticle; Wastewater treatment

1. Introduction

Limited supply of phosphorus (P) reserves and the increasing demand for food production have created a strong demand for P fertilizers. Global P depletion is one of the important challenges in the 21st century [1]. However, runoff from fields and feedlots introduces large quantities of P-containing fertilizers and animal wastes into surface waters, causing water pollution and eutrophication. Such runoff is a danger for the denizen of water and the whole ecosystem on a broader prospective. Eutrophication caused by municipal and industrial wastewaters was reported even at low concentrations of P (less than 1 mg/L) [2]. In order to control algal growth, the US EPA water quality criteria stated that phosphate should not exceed 0.05 mg/L for streams discharging into lakes or reservoirs, 0.025 mg/L within a lake or reservoir, and 0.1 mg/L for streams or flowing waters not discharging into lakes or reservoirs [3]. Improved management strategies and treatment technologies are highly desired in order to reduce agricultural runoff and to capture and recycle P before it reaches water bodies.

Many approaches have been developed to remove dissolved phosphate from wastewaters prior to their discharge into natural water bodies and runoff, including physical, chemical, and biological treatment methods [4–6]. Typically, phosphate is separated from wastewaters by adding Al-, Fe-, or Ca-based coagulants and allowing the precipitates to settle out. A common drawback of this coagulation process is the high costs associated with the use of metal salts and the treatment of the remaining sludge.

* Corresponding author.

The enhanced biological phosphorus removal (EBPR) process utilizes polyphosphate-accumulating organisms (PAO) to take up and polymerize inorganic phosphate to produce polyphosphate (polyP). P level of lower than 0.11 mg/L can be achieved in the effluents after the EBPR treatment of municipal wastewater [7]. However, the performance of EBPR can be dramatically reduced due to many environmental and operating factors, making this process unstable. In addition, the inability to isolate the responsible microorganisms in EBPR and to verify their biochemical metabolism appeared to limit the development of a better understanding of the operating metabolic pathways and the characterization of the entire microbial ecology of the systems [8], thus hampering further improvement of the EBPR system.

Adsorption has attracted increasing interests for phosphate removal from wastewater due to the easiness of design and operation and no additional production of sludge. This method has also been considered as an effective approach for recycling P from wastewater effluents. Over the past decade, various adsorbents have been developed for phosphate removal from wastewaters including agricultural waste and by-products [9], anion-exchange resins [10–12], iron-oxide based adsorbents [13], aluminum-containing materials [14–16], and layered double hydroxides [17–19]. However, additional filtration or centrifugation steps are likely needed for the separation of sorbents from aqueous solutions.

Magnetic nanomaterial-based sorbents are very attractive due to their high surface area and facile solid-liquid separation under an applied magnetic field. Their surface areas per unit volume can be on the order of 5×10^7 m^2/m^3 for a 10% dispersion of 15-nm particles [20]. Adsorption of phosphate onto amine functionalized magnetic nanoparticles through electrostatic attraction has been reported [21]. However, the simple electrostatic adsorption might suffer from the interference of co-existing anions in wastewater. Core shell material with Fe_3O_4 as core (~ 600 nm diameter) and ZrO_2 as shell (~ 10 nm thickness) have also been used to remove phosphate, with adsorption capacities ranging from 8 to 39 mg P/g [22, 23].

In this study, a unique and inexpensive sorbent, aluminum-doped magnetic nanoparticles (Al-MNP), was synthesized and explored for its phosphate removal properties. The synthesis method was simple and scalable, and the prepared material had a high value of saturation magnetization, indicating the easiness of magnetic separation of the nanoparticles from the liquid phase. The Al-MNP also showed high adsorption capacity toward phosphate removal.

2. Materials and methods

2.1. Chemicals and materials

2.1.1. Materials

Ammonium hydroxide (NH_3OH), ferrous chloride ($FeCl_2$), ferric chloride ($FeCl_3$), hydrochloric acid (HCl), nitric acid (HNO_3), aluminum sulfate ($Al_2(SO_4)_3$), monopotassium phosphate (KH_2PO_4), sodium chloride (NaCl), sodium nitrate ($NaNO_3$), sodium sulfate (Na_2SO_4), and sodium hydroxide (NaOH) were obtained from Sigma Aldrich (St. Louis, MO, USA) and used as received. ICP standards for Fe, Al, and P were purchased from High-Purity Standards (Charleston,

SC, USA). Poultry rinsing wastewater was obtained by rinsing a whole bird carcass, purchased at a local grocery store, in 400 ml of DI water. Wastewater samples after primary and secondary treatment were collected from local municipal wastewater treatment plants.

2.2. Synthesis and characterization

2.2.1. Preparation of aluminum-doped magnetic nanoparticles

A diluted NH_3OH solution at pH 12 was purged with argon and heated to 90°C for 1 h. Then, a stoichiometric mixture of $FeCl_2/FeCl_3/Al_2(SO_4)_3$ was added drop-wise into the ammonium solution. The mixture was refluxed for 2 h with argon purging. The system was then cooled to room temperature, and the black precipitates at the bottom of flask were collected with a magnet (DynaMag-50, Life Technology) and washed three times with DI water. The final product was re-suspended in DI water for storage.

2.2.2. Material characterization

X-ray diffraction (XRD) data were collected with a Bruker D8 Advanced X-Ray Diffractometer with a copper Kα source over a 15–85° 2θ range. Magnetic measurements were performed using a Quantum Design MPMS-5S SQUID magnetometer. Particles were immobilized in icosane ($C_{20}H_{42}$, Aldrich) for hysteresis measurements. High resolution scanning transmission electron microcopy imaging and elemental mapping were conducted on Hitachi HD-2700 with Oxford XMax EDX detector. Scanning electron microscopy (SEM) imaging and elemental mapping were performed on Hitachi 8230 equipped with Oxford XMax EDX detector. The composition of the Al-MNP was also determined by inductively coupled plasma – optical emission spectrometry (ICP-OES). For this procedure, a known amount of nanoparticles was digested by concentrated HNO_3 in a Parr bomb at 200°C for 2 h. Serial dilutions were performed in 2% HNO_3. Elemental analysis for Fe, Al, and P was performed on Perkin Elmer Optima 8000 ICP-OES. P levels in water samples were also measured by ICP-OES.

2.2.3. Synchrotron x-ray absorption spectroscopy (XAS) analysis

Synchrotron-based X-ray absorption near edge structure (XANES) analysis was conducted at P K-edges to investigate the local coordination environment of P during phosphate sorption onto the pure and Al-doped MNP. XANES spectra were also collected on two reference compounds $AlPO_4$ (VWR) and $FePO_4$ (Aldrich). Phosphate sorption samples were obtained by reacting 3 mg of pure or Al-MNP with 30 mL of 30 ppm phosphate solution under constant shaking conditions for 2 h. At the end of reaction, an external magnet was used to separate the adsorbent from the liquid phase, followed by DI rinse (three times). The wet pastes were stored at –20°C and only thawed before XAS data collection. Data collection was conducted in fluorescence mode at beam line 14-3 at the Stanford Synchrotron Radiation Lightsource (SSRL), Menlo Park, CA. Reference samples were grounded into fine powders and brushed evenly onto P-free Kapton tapes. Excess powders were blown off to achieve a homogeneous thin film.

For phosphate sorption samples, a thin layer of the thawed wet paste were directly mounted onto Kapton tapes and covered by a layer of 3-mm polypropylene film to avoid evaporation. The sample-loaded tapes were then mounted to a sample holder. The sample chamber was maintained under a He atmosphere at room temperature, and the spectra were collected in fluorescence mode using a PIPS detector. Energy calibration used AlPO$_4$ by setting the edge position (peak maxima of the first derivative) to be 2152.8 eV. Spectra for this reference sample were periodically collected to monitor possible energy shifting, which was not observed during data collection. XANES spectra were collected at energy ranges from 2,100 to 2,485 eV. Multiple scans were collected for each sample averaged, and normalized for further analysis. Data analysis was performed using the software SIXPack [24] and Ifeffit [25].

2.3. Phosphate adsorption experiments

2.3.1. Adsorption isothermal experiment

A phosphate stock solution with a concentration of 1,000 ppm was prepared by dissolving KH$_2$PO$_4$ in DI water. A volume of 30 mL of phosphate with concentrations ranging from 1 to 40 ppm was prepared in DI water in a 50 mL centrifuge tube. Then, 5 mL of the solution were taken out as a positive control for P level measurement. And then, 3 and 6 mg of Al-MNP, respectively, were added into the phosphate solutions and shaken on a wrist shaker overnight. Then, an external magnet was used to separate the adsorbent from the liquid phase. The supernatant was collected and the concentration of P in supernatant was measured by ICP-OES. The adsorption capacity of phosphate by Al-MNP can be expressed as follows:

$$q_e = (C_o - C_e)\frac{v}{m} \tag{1}$$

where q_e is the adsorption capacity at equilibrium (mg/g), C_0 is initial concentration of solution (mg/L), C_e is the concentration at the adsorption equilibrium (mg/L), V is the volume of water sample (L) and m is the mass of the sorbent (g). Both Langmuir and Freundlich models were tested for fitting the sorption isotherms. The Langmuir equation is expressed as:

$$\frac{C_e}{q_e} = \frac{1}{q_m}C_e + \frac{1}{K_L q_m} \tag{2}$$

where q_m is the maximum adsorption capacity (mg/g), and K_L is the Langmuir adsorption constant (L/mg). If the adsorption system followed a Langmuir adsorption model, then a plot of C_e/q_e vs. C_e would produce a straight line from which the constants q_m and K_L could be evaluated.

The Freundlich adsorption isotherm is represented by the following equation:

$$\ln q_e = \ln K_F + \frac{1}{n}\ln C_e \tag{3}$$

where K_F is a Freundlich constant in (mg/g) (L/mg)$^{1/n}$, and n is a Freundlich constant representing the adsorption intensity. If the adsorption system followed the Freundlich model, then

a plot of $\ln q_e$ vs. $\ln C_e$ would give a straight line from which constants K_F and n could be evaluated.

2.3.2. Phosphate removal studies

Phosphate removal experiments were performed in 10 mL of 10 ppm phosphate solutions with 0.1 M NaNO$_3$ as background electrolyte. Then, 3 mg of Al-MNP was added into the phosphate solution and mixed for 30 min using a wrist shaker. A magnet was used to attract the particles to the side of the tube, and the supernatant was collected for ICP analysis. For experiments involving variable pH, the pH values were adjusted by adding diluted HNO$_3$ or NaOH. Phosphate removal efficiency at time t was calculated as:

$$\%\text{removal} = \frac{C_o - C_t}{C_o} \times 100\% \tag{4}$$

2.4. Dopant leaching test

To determine whether metals from the nanoparticles were leached back into solution, 3 mg of Al-MNP was added into 10 mL of 10 ppm phosphate solution and the suspension was shaken for 30 min using a wrist shaker. The supernatant was collected after magnetic separation and analyzed for Al and Fe concentrations by ICP-OES.

2.5. Al-MNP nanoparticle regeneration

After conducting the Al-MNP in a typical phosphate removal experiment, phosphate-loaded Al-MNPs were soaked in 0.05 M Al$_2$(SO$_4$)$_3$ for 5 min. The supernatant and regenerated Al-MNPs were magnetically separated, followed by rinsing twice with 0.1 M NaNO$_3$.

3. Results and discussion

3.1. Characterization of pure and Al-MNPs

The XRD patterns of both pure and Al-doped magnetite (Fe$_3$O$_4$) magnetic nanoparticles are shown in Fig. 1.
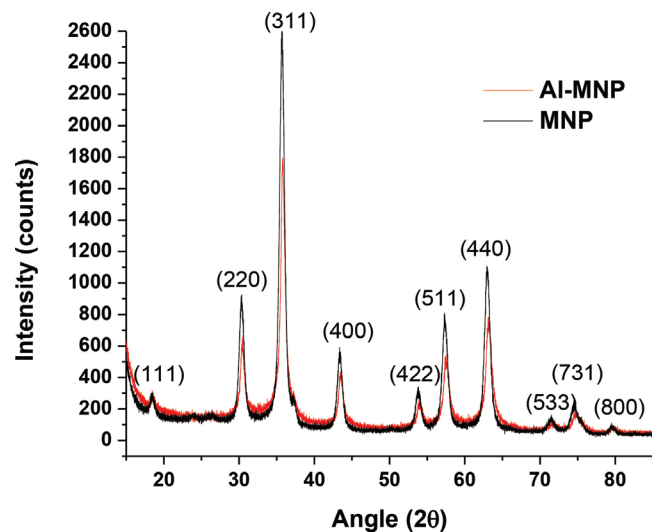

Fig. 1. X-ray diffraction patterns of pure and Al-doped magnetite.

The peaks centered at 2θ = 31°, 36°, 44°, 58° and 63° can be indexed as the (220), (311), (400), (511) and (440) planes of magnetite, in agreement with the standard magnetite JCPDS card (card no. 19-0629). However, slight peak shifts were observed for Al-MNP. Rietveld refinement was performed to extract the lattice constant and averaged crystallite size, and the results indicated that the lattice constant was reduced from 8.358Å in pure MNP to 8.334Å in Al-MNP and the grain size was also reduced from 14.24 nm in pure MNP to 9.88 nm in Al-MNP. The size of the prepared Al-MNP was confirmed to be around 10 nm, as shown in the SEM picture in Fig. 2.

Synthesis of magnetite in the presence of Al was previously reported to produce Fe_3O_4–$FeAl_2O_4$ solid solution [26].
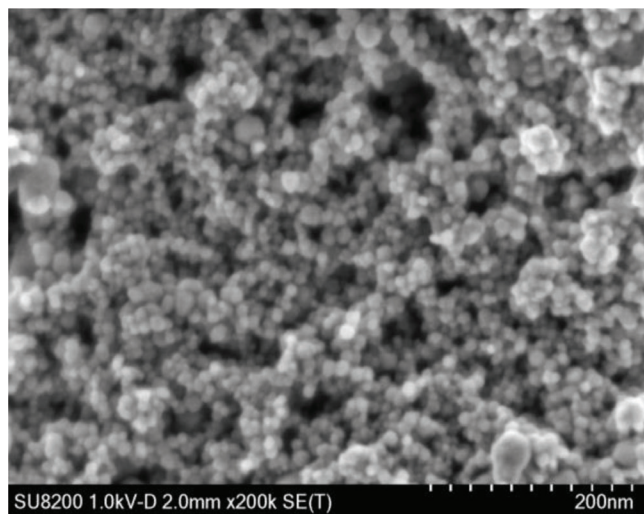

Fig. 2. SEM picture of the prepared Al-MNP.

The lattice constant of the doped Fe_3O_4–$FeAl_2O_4$ solid solution as a function of $FeAl_2O_4$ concentration X (mol%) at room temperature was described by the following Vegard's equation [27]:

$$L_d\left(\mathring{A}\right) = 8.391 - 0.00190X - 0.5X^2 \times 10^{-5}$$

Our 8.334 Ålattice constant of the Al-MNP corresponded to 30% of $FeAl_2O_4$ in the solid solution. SEM-EDX and ICP-OES determined Al:Fe ratios were 0.30 and 0.31, respectively, corresponding to 34% of $FeAl_2O_4$ in the solid solution. The less amount of $FeAl_2O_4$ as determined by XRD might suggest that small amounts of Al ions remained as amorphous Al (oxy)hydroxide phase(s) in the doped nanoparticles. High resolution transmission electron microscopy (HRTEM) with energy dispersive spectroscopy (EDX) was employed to examine Al distribution in the obtained Al-MNP nanoparticles. As shown in Fig. 3, Al exhibited a uniform distribution as that of Fe, suggesting structural incorporation. The lattice fringe spacing between two adjacent crystal planes of the nanoparticle was 0.485 nm in the HRTEM image, corresponding to the (111) lattice plane of a single-phase Fe_3O_4 [28].

The magnetic moments of both pure and Al-MNP were measured and compared as a function of applied magnetic field at a constant temperature of 300 K (Fig. 4). Both types of nanoparticles show superparamagnetism without hysteresis and remnant magnetization at room temperature. The saturation magnetization was found to be 77 emu/g for pure MNP and 26.3 emu/g for Al-MNP. The reduced magnetization for Al-MNP could be explained by the replacement of Fe^{3+} by nonmagnetic Al^{3+} in octahedral sites in a face-centered cubic lattice structure [26].
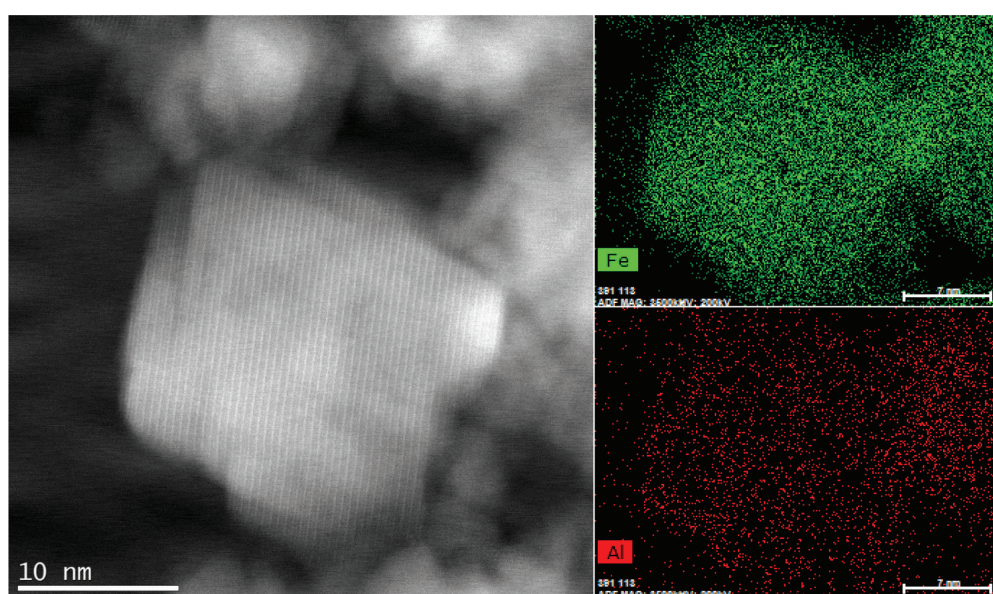

Fig. 3. High resolution transmission electron microscopic photograph of Al-MNP particle (left) and EDX mapping of Fe and Al distribution on the particle (left).
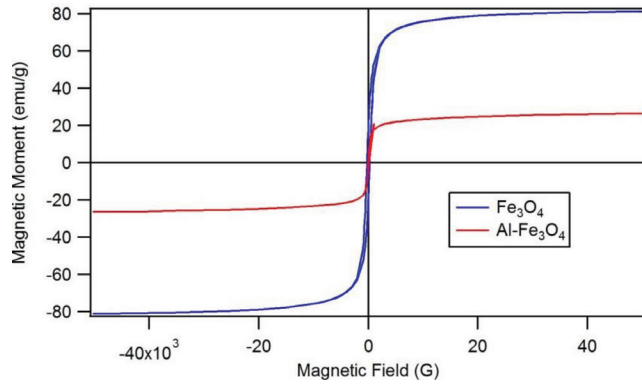
Fig. 4. Magnetic moment measurements for pure and Al-doped MNP.

3.2. Adsorption kinetic studies

To determine phosphate sorption kinetics, 3 mg of Al-MNP was mixed with 10 mL of phosphate at concentrations of 10, 20 and 30 ppm (typical municipal waste water contains 10 to 30 ppm phosphate [29]), and phosphate uptake was measured at various time points (Fig. 5). The initial adsorption was fast, with ~75% of phosphate removed within the first 30 min, and greater than 90% of phosphate removal can be achieved in 2 h. The fast removal rate can be contributed to the high surface area of the MNP and the ease of dispersion into the liquid stream for better mixing with contaminants. Three well-known kinetic models, including the pseudo-first-order model, pseudo-second-order models, and the intraparticle diffusion model, were used to fit of the phosphate removal kinetic data. The pseudo-first-order model was given as:

$$\ln\left(q_e - q_t\right) = \ln q_e - k_1 t \qquad (5)$$

The pseudo-second-order kinetic model was given as:

$$\frac{t}{q_t} = \frac{1}{k_2 q_e^2} + \frac{1}{q_e} t \qquad (6)$$

The intraparticle diffusion kinetic model is given as:

$$q_t = k_d t^{1/2} + C \qquad (7)$$

where q_t is the amount of phosphate removed at time t(mg/g), q_e is the adsorption capacity at equilibrium (mg/g), k_1 is the pseudo-first-order rate constant (min^{-1}), k_2 is the pseudo-second-order rate constant (g/(mg·min)), kd is the intraparticle diffusion rate constant (mg/(g·min$^{0.5}$)), and t is the contact time (min). Plots of log($q_e − q_t$) vs. t, t/q_t vs. t, and q_t vs. $t^{0.5}$ generated the rate constants, q_e and the correlation coefficients R^2, which were compared in Table 1.

The most likely kinetic model for the adsorption of phosphate on Al-MNP was the pseudo-second-order model. Although the correlation coefficient for pseudo-first-order was greater than 0.9, there was a large difference between the experimental and theoretical adsorbed masses at equilibrium. This result indicated that the adsorption of
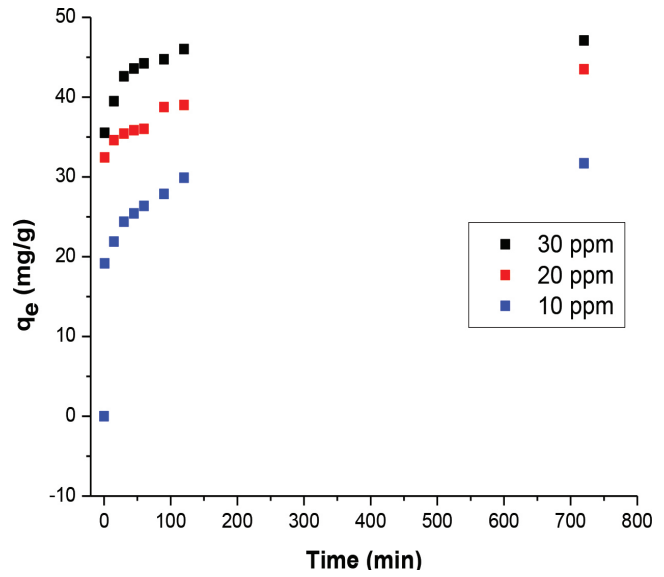

Fig. 5. Effect of contact time on the phosphate removal: 3 mg Al-MNP were added into 10 ml of 10, 20, and 30 ppm phosphate solution for the tests.

Table 1
Kinetic parameters for the adsorption of phosphates onto Al-MNP

Initial phosphate concentrations (mg/L)		10	20	30
Experimental q_e (mg/g)			31.7	43.5	47.1
Pseudo-first-order model	k_1 (min^{-1})	0.015	0.007	0.018
	q_e (mg/g)	12.52	10.59	9.49
	R^2	0.972	0.93	0.94
Pseudo-second-order mode	k_2 (g/(mg·min))	0.177	0.0027	0.0065
	q_e (mg/g)	30.3	43.86	47.62
	R^2	0.992	0.999	0.999
Intraparticle diffusion model	k_d (mg/(g·min$^{0.5}$))	1.067	33.21	39.65
	R^2	0.992	0.91	0.498

phosphates onto Al-MNP was not an ideal pseudo-first-order reaction. The intraparticle diffusion model describes the adsorption processes where the rate of adsorption depends on the speed at which the adsorbate diffuses towards adsorbent. We obtained a better fit using this model at a low phosphate concentration, indicating some degree of diffusion-controlled step involved during the phosphate removal process at low phosphate levels. However, at higher phosphate concentrations, the rate limiting step became surface adsorption.

For the pseudo-second-order model, the correlation coefficients for all initial phosphate concentrations were higher than 0.99. In addition, the difference between the experimental and theoretical adsorbed masses at equilibrium was very small (less than 1%), indicating that the adsorption of
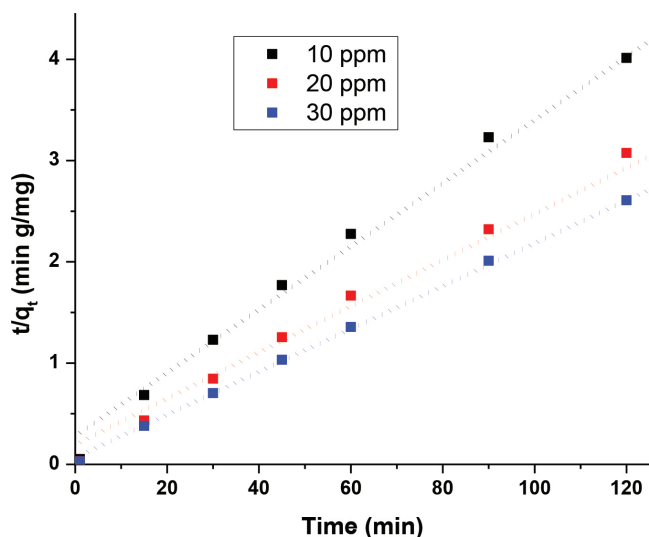
Fig. 6. Pseudo-second-order fitting of phosphate removal data obtained in Fig. 5.

phosphate on Al-MNP could be a pseudo-second-order reaction. In this model, the rate-limiting step was the surface adsorption that involved chemisorption, where the phosphate removal from a solution was due to physicochemical interactions between the two phases. The pseudo-second-order model of phosphate removal was plotted as a function of time in Fig. 6.

3.3. pH effects

The effect of pH on phosphate removal was also examined (Fig. 7). These results showed that the removal efficiency was independent of the pH for pH 4 to 9. At pH 10, phosphate removal efficiency dropped from 95% to about 59%, likely due to the leaching of doped Al ions from Al-MNP as determined by ICP-OES analysis of the solution.

3.4. Adsorption interference studies

We also tested the potential influence of other common constituents in wastewaters on P removal by Al-MNP. Phosphate removal was assessed in the presence of 10 mg/L chloride (Cl^-), nitrate (NO_3^-), and sulfate (SO_4^{2-}). The effects of these coexisting anions on phosphate removal were shown in Fig. 8. Results showed that the presence of these anions only slightly reduced phosphate adsorption by 5% to 7%, suggesting that the Al-MNP was selective to phosphate adsorption. Poultry rinse water, which contained high level of organic matters, fat, and proteins, was also tested for phosphate removal. The phosphate level in the rinsing water was around 30 mg/L. The rinse water was filtered through a 1-μm syringe filter to prevent clogging during ICP measurements, and then diluted to have a final phosphate level of 10 ppm for direct comparison with the other experiments. The data can also be found in Fig. 8. All of the tests performed indicated that the presence of additional anions, as well as organic materials from poultry rinse, did not interfere with the phosphate removal efficacy.
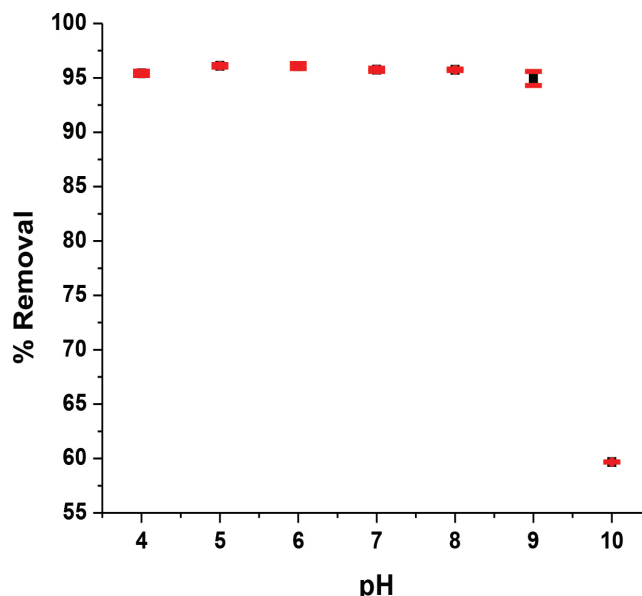

Fig. 7. Effect of pH on phosphate removal: pH was adjusted using diluted HCl and NaOH. Loss of Al from Al-MNP particle at pH 10, confirmed by ICP analysis, caused a lower phosphate binding capability.
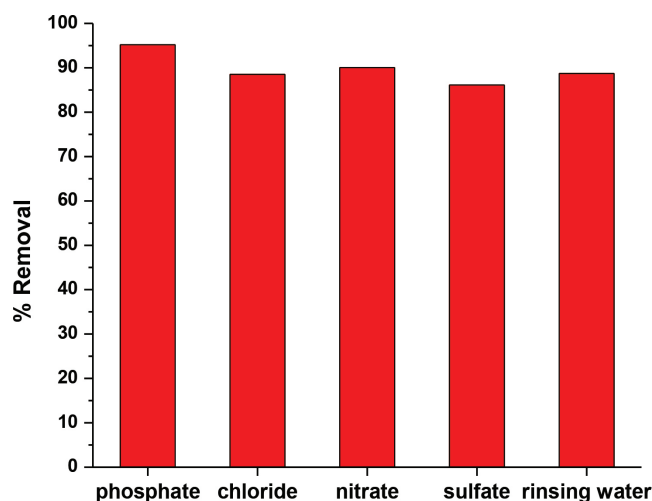

Fig. 8. Effect of co-existence of other anions on phosphate removal: only slightly reduced efficacies were observed when other common anions and organics were presented in water samples.

3.5. Adsorption isotherm studies

The sorption isotherm was examined to understand how phosphate anions distribute themselves between liquid and solid phases at equilibrium. The most common adsorption models are the Langmuir model (corresponding to a monolayer of homogeneous adsorbent surface) and the Freundlich model (corresponding to a heterogeneous adsorbent surface). Table 2 summarized the parameters obtained from the curve fitting with two models. Clearly, the experimental data fitted better with the Langmuir model of a monolayer homogeneous adsorbent surface, and the maximum adsorption capacity was greater than 100 mg/g. These results surpassed

Table 2
Adsorption isotherm parameters with Langmuir and Freundlich models

Amount of adsorbent	Langmuir model				Freundlich model		
	q_m (mg/g)	K_L (L/mg)	R_L	R^2	K_F (mg/g)(L/mg)$^{1/n}$	n	R^2
3 mg Al-MNP	102.15	1.09	0.022	0.988	43.82	2.88	0.806
6 mg Al-MNP	81.31	1.09	0.022	0.996	32.07	2.57	0.444

Table 3
Comparison of adsorption capacity of Al-MNP with other magnetic adsorbents

Adsorbent	Maximum adsorption capacity (mg PO$_4$/g)	Reference
Diatom frustules coated on Fe$_3$O$_4$	4.89	[30]
Core–shell Fe$_3$O$_4$@LDHs composite	26.5–36.9	[31]
Magnetic iron oxide nanoparticles	5.03	[32]
Fe–Zr binary oxide	13.65	[33]
Tetraethylenepentamine-coated Fe$_3$O$_4$	81–102	[21]
Magnetite modified with aluminum/silica	25.64	[34]
Polyacrylamide coated Fe$_3$O$_4$	28.95	[35]
ZrO$_2$ shell and magnetite core (Fe$_3$O$_4$@mZrO$_2$)	39.1	[23]
Mesoporous rodlike NiFe$_2$O$_4$	39.3	[36]
Al-Fe$_3$O$_4$	102.15	Our work

the commercially available adsorbents as mentioned in the literature [9] and the reported magnetic adsorbents for phosphate, as shown in Table 3.

The increased adsorption capacity originated from the doped Al. The pure MNP had a much lower capacity for phosphate adsorption compared with Al-MNP. In addition, the treated Al-MNP at a higher pH lost its phosphate binding capability as a result of the loss of Al from the doped particle. We have also tried to dope magnesium (Mg), calcium (Ca), and lanthanum (La)to the Fe$_3$O$_4$ magnetic nanoparticles, but did not observe much enhanced adsorption behavior.

The Langmuir constant K_L is related to the standard free energy of adsorption (ΔG°) and indicates the phosphate binding affinity of the adsorbent. A high K_L value indicates greater affinity for phosphate adsorption by an adsorbent. To determine whether the adsorption is favorable, the essential characteristics of the Langmuir equation can be expressed in a dimensionless separation factor or equilibrium parameter, R_L, as defined in Eq. (8), where C_0 is the highest initial phosphate concentration (mg/L). The factor R_L was within the range of 0 and 1.0, suggesting the favorability of phosphate

adsorption onto the Al-MNP. In addition, the calculated n value in the Freundlich model was greater than 1, indicating a favorable adsorption [31].

$$R_L = \frac{1}{1 + K_L C_o} \qquad (8)$$

3.6. Phosphate uptake mechanism

P K-edge XANES analysis was conducted to elucidate the mechanism(s) for the enhanced phosphate uptake on Al-MNP as compared with MNP. The XANES spectra of P sorbed MNP and FePO4 both exhibit a unique pre-edge feature at ~2150 eV (dashed line in Fig. 9). The presence of this pre-edge peak has been previously observed for phosphate minerals containing Fe(III) species, such as heterosite and strengite [37–41]. As a comparison, Al-containing phosphate minerals, such as AlPO4 in our system, do not have such pre-edge peak [37]. Therefore, in a simple controlled system such as ours, the presence and amplitude of this pre-edge peak can be used to identify the relative contribution of P-Fe association. Previous studies have demonstrated the formation of inner-sphere complexes (e.g., bond formation between phosphate tetrahedral and surface Fe atoms) during the sorption of phosphate onto Fe and Al oxide minerals [40–43]. The intensity of the pre-edge feature can be correlated with the relative proportion of phosphate bonded with Al(III) vs. Fe(III) [40, 41, 43]. Therefore, the much lower intensity of this pre-edge feature in the P sorbed Al-MNP sample suggests that large amount of phosphate was bonded to surface Al sites vs. Fe sites.

3.7. Metal leaching and particle regeneration

We have observed that the doped Al was securely incorporated into the magnetite structure. Regular rinsing did not remove Al from the doped magnetic nanoparticles. This observation was confirmed by examining the metal levels in the liquid phase after phosphate removal. In a typical phosphate removal experiment, after 1-min magnetic separation of the particles from the liquid phase, the supernatant only contained 15 ppb Al and 30 ppb Fe, meaning 99.94% of magnetic particles were separated from the liquid phase. The remaining Al and Fe in the treated water originated from the residual magnetic nanoparticles in the liquid phase.

To lower the operation cost, the regeneration of Al-MNP was explored. It was discovered that phosphate adsorbed onto the Al-MNP can easily be stripped off through a competitive binding between the Al on the Al-MNP and Al in the solution. Using a 0.05 M Al^{3+} solution, the adsorbed
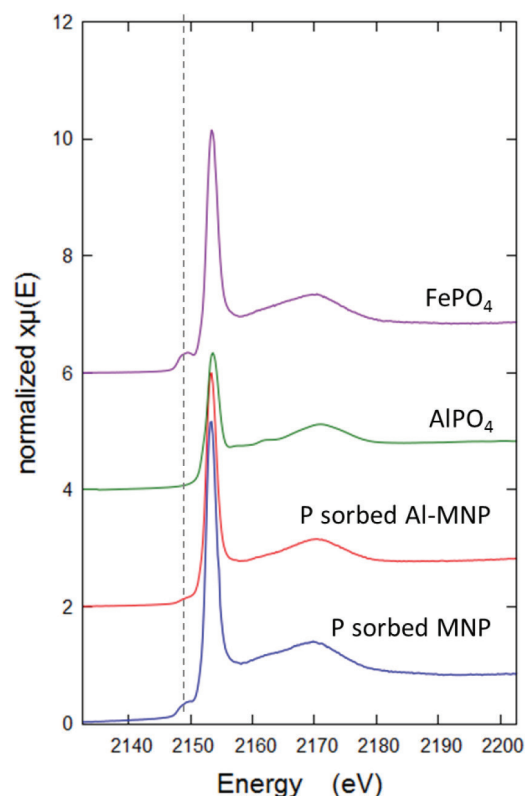
Fig. 9. P K-edge XANES spectra of phosphate sorbed pure MNP and Al-MNP, as well as reference compounds AlPO4 and FePO4: dashed line highlights the pre-edge peak associated with P-Fe coordination.
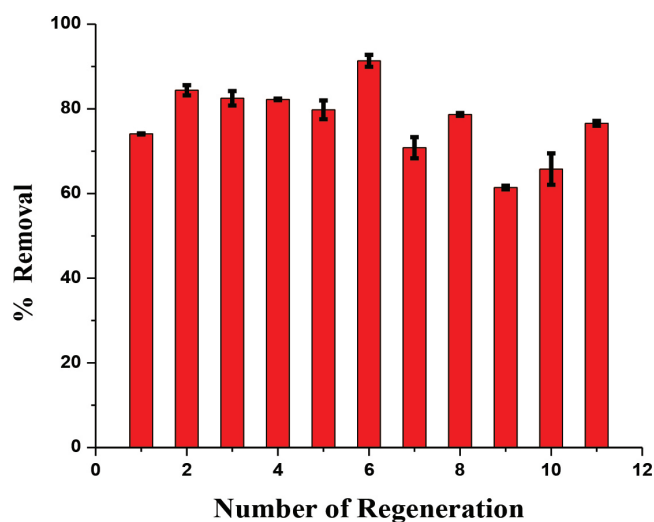

Fig. 10. 3 mg of Al-MNP was regenerated and reused for 11 times in 10 ml of 10 ppm phosphate removal.

phosphate was removed from the Al-MNP. The regenerated Al-MNP were then rinsed twice with 0.1 M $NaNO_3$ to remove any loosely attached Al on the particle before being used again for phosphate removal. Fig. 10 showed the regeneration capability of Al-MNP. It was clear that regenerated Al-MNP did not lose much phosphate binding capability

Table 4
Phosphate removal in wastewater samples

Sample type	Amount of adsorbent (mg)	Phosphate level before (ppm)	Phosphate level after (ppm)	Phosphate removal (%)
Tap water	3	1.45 ± 0.02	0.262 ± 0.01	82%
Primary effluent	10	26.4 ± 0.35	2.01 ± 0.03	92.3%
Secondary effluent	3	0.95 ± 0.04	0.17 ± 0.002	82%

after 11 cycles of regeneration. Aluminum phosphate in the regeneration solution can later be converted to phosphate fertilizers.

3.8. Wastewater treatment

The Al-MNPs were tested for phosphate removal on tap water, primary wastewater effluent, and secondary wastewater effluent. Without any additional pretreatment, these waters were directly treated with Al-MNP to examine the matrix effect on the phosphate removal efficacy. Table 4 summarizes the phosphate levels before and after the treatment. Due to the high phosphate concentration in the sample collected from primary effluent, 10 mg of Al-MNP was used; 3 mg was used for both tap water and secondary effluent water. Great phosphate reductions (above 80%) were obtained in all three water samples within 30 min. Although the phosphate level in the treated primary effluent sample was still high (2 ppm), either adding more adsorbents or performing a secondary Al-MNP treatment would reduce the phosphate level in the primary effluent to below 1 ppm. The phosphate level in tap water was greater than the secondary effluent because blended phosphates (1 to 5 ppm) are typically added to the drinking water as a corrosion inhibitor to prevent the leaching of lead and copper from pipes and fixtures [44].

4. Conclusion

We have successfully developed a simple and low-cost method to remove phosphate from wastewater streams through the use of unique aluminum-doped magnetic nanoparticles. Aluminum-doped magnetic nanoparticles were synthesized using a co-precipitation method. Structure and composition analysis of the prepared magnetic nanoparticles indicated an inverse spinal structure with a composition of $FeAl_{0.75}Fe_{1.25}O_4$. These novel particles not only have a great adsorption capacity to phosphate. They also have an excellent selectivity for phosphate removal, even in the presence of other anions and organic materials such as fat and proteins. This property allows the particles to be used for a variety of wastewater treatments, as supported by the high levels of removal in poultry rinse water, tap water, and local municipal wastewater. Used Al-MNP can be regenerated for multiple cycles through a competitive binding chemistry by dispersing the particles in an aluminum sulfate solution. Therefore, the overall costs for phosphate removal are fairly low. This research demonstrated that the doped magnetic

nanoparticles can be used as a promising adsorbent for phosphate removal in wastewaters. Although an external magnet separates the majority of the magnetic nanoparticles from the wastewater stream, there will be always some nanomaterials left in the liquid phase. The fates of the synthesized nanomaterials need to be investigated in order to fully explore the nanomaterials based wastewater treatment technologies.

Acknowledgements

References

[1] S.M. Heilmann, J.S. Molde, J.G. Timler, B.M. Wood, A.L. Mikula, G.V. Vozhdayev, E.C. Colosky, et al., Phosphorus reclamation through hydrothermal carbonization of animal manures, Env. Sci. Technol., 48 (2014) 10323–10329.

[2] D. Correll, The role of phosphorus in the eutrophication of receiving waters: a review, J. Env. Qual., 27 (1998) 261–266.

[3] EPA, *Quality Criteria for Water, Office of Water Regulations and Standards*, Washington DC, 1986.

[4] C. Pratt, S.A. Parsons, A. Soares, B.D. Martin, Biologically and chemically mediated adsorption and precipitation of phosphorus from wastewater, Curr. Opin. Biotech., 23 (2012) 890–896.

[5] G.T. Daigger, H.X. Littleton, Simultaneous biological nutrient removal: a state-of-the-art review, Water Env. Res., 86 (2014) 245–257.

[6] W.Q. Guo, H.C. Luo, S.S. Yang, Q.L. Wu, S.M. Peng, Emerging technologies for phosphorus removal and recovery: a review, Appl. Mech. Mater., 507 (2014) 702–706.

[7] I. Kamika, M. Coetzee, B. Mamba, T. Msagati, M. Momba, The impact of microbial ecology and chemical profile on the enhanced biological phosphorus removal (EBPR) process: a case study of Northern Wastewater Treatment Works, Johannesburg, Int. J. Environ. Res. Public Health, 11 (2014) 2876–2898.

[8] M. Henze, *Biological wastewater treatment: principles, modelling and design*, IWA publishing, 2008.

[9] T.A.H. Nguyen, H.H. Ngo, W.S. Guo, J. Zhang, S. Liang, D.J. Lee, P.D. Nguyen, X.T. Bui, Modification of agricultural waste/by-products for enhanced phosphate removal and recovery: potential and obstacles, Bioresource Technol., 169 (2014) 750–762.

[10] J. Sun, X. Li, Y. Quan, Y. Yin, S. Zheng, Effect of long-term organic removal on ion exchange properties and performance during sewage tertiary treatment by conventional anion exchange resins, Chemosphere, 136 (2015) 181–189.

[11] A. Sendrowski, T.H. Boyer, Phosphate removal from urine using hybrid anion exchange resin, Desalination, 322 (2013) 104–112.

[12] Y.-S. Kim, Y.-H. Lee, B. An, S.-A. Choi, J.-H. Park, J.-S. Jurng, S.-H. Lee, J.-W. Choi, Simultaneous removal of phosphate and nitrate in wastewater using high-capacity anion-exchange resin, Water Air Soil Poll., 223 (2012) 5959–5966.

[13] P. Wilfert, P.S. Kumar, L. Korving, G.-J. Witkamp, M.C.M. van Loosdrecht, The relevance of phosphorus and iron chemistry to the recovery of phosphorus from wastewater: a review, Env. Sci. Technol., (2015).

[14] D.A. Georgantas, H.P. Grigoropoulou, Orthophosphate and metaphosphate ion removal from aqueous solution using alum and aluminum hydroxide, J. Colloid Interface Sci., 315 (2007) 70–79.

[15] D. Guaya, C. Valderrama, A. Farran, C. Armijos, J.L. Cortina, Simultaneous phosphate and ammonium removal from aqueous solution by a hydrated aluminum oxide modified natural zeolite, Chem. Eng. J., 271 (2015) 204–213.

[16] J. Xie, Y. Lin, C. Li, D. Wu, H. Kong, Removal and recovery of phosphate from water by activated aluminum oxide and lanthanum oxide, Powder Technol., 269 (2015) 351–357.

[17] Y. Xu, H. Lv, G. Qian, J. Zhang, J. Zhou, Dual removal process of phosphate on Ca-layered double hydroxide with substitution of Fe for Al, J. Hazard. Toxic Radioact., 18 (2014) A4014001.

[18] C. Novillo, D. Guaya, A. Allen-Perkins Avendaño, C. Armijos, J.L. Cortina, I. Cota, Evaluation of phosphate removal capacity of Mg/Al layered double hydroxides from aqueous solutions, Fuel, 138 (2014) 72–79.

[19] M. Zhang, B. Gao, J. Fang, A.E. Creamer, J.L. Ullman, Self-assembly of needle-like layered double hydroxide (LDH) nano-crystals on hydrochar: characterization and phosphate removal ability, RSC Adv., 4 (2014) 28171–28175.

[20] D.A.J. Seyda Bucak, P.E. Laibinis, T.A Hatton, Protein separations using colloidal magnetic nanoparticles, Biotechnol. Prog., 19 (2003) 477–484.

[21] H. Shen, Z. Wang, A. Zhou, J. Chen, M. Hu, X. Dong, Q. Xia, Adsorption of phosphate onto amine functionalized nano-sized magnetic polymer adsorbents: mechanism and magnetic effects, RSC Adv., 5 (2015) 22080–22090.

[22] W. Wang, H. Zhang, L. Zhang, H. Wan, S. Zheng, Z. Xu, Adsorptive removal of phosphate by magnetic Fe3O4@C@ZrO2, Colloids Surf. A Physicochem. Eng. Asp., 469 (2015) 100–106.

[23] A. Sarkar, S.K. Biswas, P. Pramanik, Design of a new nano-structure comprising mesoporous ZrO2 shell and magnetite core (Fe3O4@mZrO2) and study of its phosphate ion separation efficiency, J. Mater. Chem., 20 (2010) 4417–4424.

[24] S. Webb, SIXpack: a graphical user interface for XAS analysis using IFEFFIT, Phys. Scripta, 2005 (2005) 1011.

[25] á. Ravel, M. Newville, ATHENA, ARTEMIS, HEPHAESTUS: data analysis for X-ray absorption spectroscopy using IFEFFIT, J. Synchrotron Radiat., 12 (2005) 537–541.

[26] Y. Okano, T. Nakamura, Hydrothermal synthesis of aluminum bearing magnetite particles, Colloids Surf. A Physicochem. Eng. Asp., 139 (1998) 279–285.

[27] Y. Kapelyushin, Y. Sasaki, J. Zhang, S. Jeong, O. Ostrovski, In-situ study of gaseous reduction of magnetite doped with alumina using high-temperature XRD analysis, Metall. Mater. Trans. B, (2015) 1–9.

[28] X.-H. Jia, H.-J. Song, C.-Y. Min, X.-Q. Zhang, One-step synthesis of Fe3O4 nanorods/graphene nanocomposites, Appl. Phys. A., 109 (2012) 261–265.

[29] M.A. Latif, C.M. Mehta, D.J. Batstone, Low pH anaerobic digestion of waste activated sludge for enhanced phosphorous release, Water Res., 81 (2015) 288–293.

[30] J. Toster, I. Kusumawardani, E. Eroglu, K.S. Iyer, F. Rosei, C.L. Raston, Superparamagnetic imposed diatom frustules for the effective removal of phosphates, Green Chem., 16 (2014) 82–85.

[31] L.-G. Yan, K. Yang, R.-R. Shan, T. Yan, J. Wei, S.-J. Yu, H.-Q. Yu, B. Du, Kinetic, isotherm and thermodynamic investigations of phosphate adsorption onto core–shell Fe3O4@LDHs composites with easy magnetic separation assistance, J. Colloid Interface Sci., 448 (2015) 508–516.

[32] S.-Y. Yoon, C.-G. Lee, J.-A. Park, J.-H. Kim, S.-B. Kim, S.-H. Lee, J.-W. Choi, Kinetic, equilibrium and thermodynamic studies for phosphate adsorption to magnetic iron oxide nanoparticles, Chem. Eng. J., 236 (2014) 341–347.

[33] F. Long, J.-L. Gong, G.-M. Zeng, L. Chen, X.-Y. Wang, J.-H. Deng, Q.-Y. Niu, et al., Removal of phosphate from aqueous solution by magnetic Fe–Zr binary oxide, Chem. Eng. J., 171 (2011) 448–455.

[34] Y.-F. Lin, H.-W. Chen, C.-C. Chang, W.-C. Hung, C.-S. Chiou, Application of magnetite modified with aluminum/silica to adsorb phosphate in aqueous solution, J. Chem. Technol. Biotechnol., 86 (2011) 1449–1456.

[35] Y.-F. Lin, H.-W. Chen, Y.-C. Chen, C.-S. Chiou, Application of magnetite modified with polyacrylamide to adsorb phosphate in aqueous solution, J. Taiwan Inst. Chem. Eng., 44 (2013) 45–51.

AQ1

AQ2

[36] Z. Jia, Q. Wang, J. Liu, L. Xu, R. Zhu, Effective removal of phosphate from aqueous solution using mesoporous rodlike NiFe2O4 as magnetically separable adsorbent, Colloids Surf. A Physicochem. Eng. Asp., 436 (2013) 495–503.

[37] E.D. Ingall, J.A. Brandes, J.M. Diaz, M.D. de Jonge, D. Paterson, I. McNulty, W.C. Elliott, P. Northrup, Phosphorus K-edge XANES spectroscopy of mineral standards, J. Synchrotron Radiat., 18 (2011) 189–197.

[38] G. Pratesi, C. Cipriani, G. Giuli, W.D. Birch, Santabarbaraite: a new amorphous phosphate mineral, Eur. J. Mineral., 15 (2003) 185–192.

[39] D. Hesterberg, W. Zhou, K.J. Hutchison, S. Beauchemin, D.E. Sayers, XAFS study of adsorbed and mineral forms of phosphate, J. Synchrotron Radiat., 6 (1999) 636–638.

[40] N. Khare, D. Hesterberg, J.D. Martin, XANES investigation of phosphate sorption in single and binary systems of iron and aluminum oxide minerals, Env. Sci. Techno., 39 (2005) 2152–2160.

[41] N. Khare, D. Hesterberg, S. Beauchemin, S.-L. Wang, XANES determination of adsorbed phosphate distribution between ferrihydrite and boehmite in mixtures, Soil. Sci. Soc. Am. J., 68 (2004).

[42] D.B. Abdala, P.A. Northrup, F.C. Vicentin, D.L. Sparks, Residence time and pH effects on the bonding configuration of orthophosphate surface complexes at the goethite/water interface as examined by Extended X-ray Absorption Fine Structure (EXAFS) spectroscopy, J. Colloid Interface Sci., 442 (2015) 15–21.

[43] Y.-T. Liu, D. Hesterberg, Phosphate bonding on noncrystalline Al/Fe-hydroxide coprecipitates, Env. Sci. Techno., 45 (2011) 6283–6289.

[44] M. Batté, B. Koudjonou, P. Laurent, L. Mathieu, J. Coallier, M. Prévost, Biofilm responses to ageing and to a high phosphate load in a bench-scale drinking water system, Water Res., 37 (2003) 1351–1361.

AQ3

Author Query

AQ1	Please provide publisher details for reference [3].
AQ2	Please provide volume number and page range for reference [13].
AQ3	Please provide page range for reference [41].